Generalized Method to Extract Carrier Diffusion Length from Photoconductivity Transients: Cases of $BiVO_4$, Halide Perovskites, and Amorphous and Crystalline Silicon

Markus Schleuning,[1,2] Moritz Kölbach,[1] Fatwa F. Abdi,[1] Klaus Schwarzburg,[1] Martin Stolterfoht,[3] Rainer Eichberger,[1] Roel van de Krol,[1,2] Dennis Friedrich,[1,*] and Hannes Hempel[4,†]

[1] *Institute for Solar Fuels, Helmholtz-Zentrum Berlin für Materialien und Energie GmbH, Hahn-Meitner-Platz 1, 14109 Berlin, Germany*

[2] *Institut für Chemie, Technische Universität Berlin, Straße des 17. Juni 124, 10623 Berlin, Germany*

[3] *Institute of Physics and Astronomy, Universität Potsdam, 14476 Potsdam-Golm, Germany*

[4] *Department Structure and Dynamics of Energy Materials, Helmholtz-Zentrum Berlin für Materialien und Energie GmbH, Hahn-Meitner-Platz 1, 14109 Berlin, Germany*

(Received 14 April 2022; revised 2 August 2022; accepted 12 August 2022; published 29 September 2022)

Long diffusion lengths of photoexcited charge carriers are crucial for high power conversion efficiencies of photoelectrochemical and photovoltaic devices. Time-resolved photoconductance measurements are often used to determine diffusion lengths in conventional semiconductors. However, effects such as polaron formation or multiple trapping can lead to time-varying mobilities and lifetimes that are not accounted for in the conventional calculation of the diffusion length. Here, a generalized analysis is presented that is valid for time-dependent mobilities and time-dependent lifetimes. The diffusion length is determined directly from the integral of a photoconductivity transient and can be applied regardless of the nature of carrier relaxation. To demonstrate our approach, photoconductivity transients are measured from 100 fs to 1 μs by the combination of time-resolved terahertz and microwave spectroscopy for $BiVO_4$, one of the most studied metal oxide photoanodes for photoelectrochemical water splitting. The temporal evolution of charge carrier displacement is monitored and converges after about 100 ns to a diffusion length of about 15 nm, which rationalizes the photocurrent loss in the corresponding photoelectrochemical device. The presented method is further validated on *a*-Si : H, *c*-Si, and halide perovskite, which underlines its potential to determine the diffusion length in a wide range of semiconductors, including disordered materials.

DOI: 10.1103/PRXEnergy.1.023008

I. INTRODUCTION

Global demand for renewable energy is driving the search for better absorber materials for photovoltaic and photoelectrochemical applications. The key parameters for carrier transport in solar or photoelectrochemical (PEC) cells are the diffusion length, L_D, for thermal motion and the drift length, L_{dr}, for drift in an electric field, E (i.e., a built-in field or an applied external voltage). In conventional semiconductors with (approximately) time-invariant mobilities, μ, and lifetimes, τ, such as Si, GaAs, and lead halide perovskites, they are given by $L_D = \sqrt{\mu\tau k_B T/q}$ and $L_{\mathrm{dr}} = \mu\tau E$, respectively, where k_B is the Boltzmann constant, T is the temperature, and q is the elementary charge [1–3].

Mobilities and lifetimes can be obtained simultaneously from photoconductivity transients that are measured by time-resolved microwave conductivity (TRMC) [4,5] and optical-pump terahertz-probe spectroscopy (OPTP) [6,7]. These techniques do not require any electrical contacts and are, therefore, especially suited for fast and noninvasive screening of novel materials. The amplitude of the photoconductivity transient can be related to the initial mobility of the photogenerated charge carriers. However, it is not obvious if the photoconductivity transient is caused by a decay in the effective mobility e.g., due to polaron formation or trapping [8,9] or by a decay in the carrier concentration due to recombination. Therefore, we herein describe an approach that does not require such a distinction and allows the calculation of the generalized

*friedrich@helmholtz-berlin.de

†hannes.hempel@helmholtz-berlin.de

diffusion length directly from the photoconductivity transient. Previous works studied photoconductivity transients mostly by either OPTP or TRMC, which probe different time windows of typically 100 fs to 2 ns and 10 ns to 100 μs, respectively. As a consequence of the mobilities and decay times being time dependent, previous OPTP studies have reported significantly shorter decay times and larger mobilities than TRMC studies on the same materials, such as Fe_2O_3, $\alpha - SnWO_4$, and $BiVO_4$ [10–12]. These differences are recognized and are usually classified as so-called "microscopic" (OPTP) and "macroscopic" (TRMC) mobilities [13–15]. The OPTP lifetimes of metal oxides are often attributed to trapping or carrier relaxation, while TRMC lifetimes are usually attributed to recombination [10,11], but the validation of these assignments remains challenging.

Here, this paradox is overcome by monitoring the entire photoconductivity transients from fs to μs by complementary OPTP and TRMC measurements. The temporal gap between them is bridged by open-cell (OC-) TRMC and sample-terminated (ST-) TRMC measurements in setups similar to those described previously in Refs. [16–18]. The higher time resolution compared to the conventional TRMC setup is achieved by manipulating the microwave resonance, using higher microwave frequencies (K_a band vs. X band), an excitation laser with a shorter pulse width, and detection electronics with higher sensitivity and bandwidth.

Applying the generalized analysis to the measured photoconductivity transient allows the temporal evolution of the mean absolute displacement of diffusing photogenerated charge carriers, which usually converges to the diffusion length, to be monitored. This analysis is demonstrated here on diverse semiconductors classes, including $BiVO_4$, amorphous hydrogenated silicon (a-Si : H), halide perovskite thin films, and a single crystalline silicon wafer (c-Si) as case studies.

II. THEORY OF THE GENERALIZED DIFFUSION LENGTH

The following generalized derivation of the diffusion length that can be applied for time-dependent lifetimes, τ, and time-dependent diffusion coefficients, D, is based on modeling unipolar diffusion and recombination by the continuity equation:

$$\frac{dn}{dt} = D\frac{d^2n}{dx^2} - \frac{1}{\tau}n, \tag{1}$$

where n is the carrier concentration and all other symbols have their usual meaning. The diffusion length, L_D, is usually defined as the average distance that photogenerated charge carriers travel from their initial position, x_0, by the time they recombine:

$$L_D = \frac{\int n_r(x, t \to \infty)|x - x_0|dx}{n_{s0}}. \tag{2}$$

The individual distances are weighted in Eq. (2) by the distribution of the recombined charge carriers, n_r, at sufficiently long times, $t \to \infty$, when all carriers recombine and are normalized by the initially induced sheet carrier concentration, $n_{s0} = \int n(x, t = 0)dx$. This distribution is given in Eq. (3) by the recombination term of the continuity equation:

$$\frac{dn_r(x,t)}{dt} = \frac{1}{\tau}n(x,t), \quad \text{with} \quad n_r(t=0) = 0. \tag{3}$$

To obtain an additional measure of how far the charge carriers diffuse at a certain time t (and not only at the point of recombination), the average absolute displacement of both recombined and remaining carriers is used here. In Eq. (4), the excited carriers contribute with their absolute displacement at the current time t, while the recombined carriers contribute with the absolute displacement at the time they recombine. At sufficiently long times, all charge carriers will recombine, and their mean absolute displacement will approach the diffusion length $L_D = \langle x(t \to \infty)\rangle$:

$$\langle x(t)\rangle = \frac{\int (n_r(x,t) + n(x,t))|x - x_0|dx}{n_{s0}}. \tag{4}$$

In the following, an analytical expression is derived that obtains the diffusion length from the photoconductivity transient. This expression is then confirmed by numerical modeling of Eqs. (1)–(4).

A charge carrier distribution that is initially situated at position x_0 is described in Eq. (5) by a Gaussian distribution with a width, w, that approaches zero (i.e., a delta function). For a constant lifetime and a constant diffusion coefficient, the solution of continuity Eq. (1) yields the evolution of the width, $w = \sqrt{2Dt}$, which represents the spreading of the root mean square displacement, $\sqrt{\langle x^2\rangle}$, of the remaining charge carriers by diffusion:

$$n(x,t) = \frac{1}{\sqrt{2w^2}}\exp\left(\frac{-(x-x_0)^2}{2w^2}\right)\exp\left(\frac{-t}{\tau}\right)$$
$$\text{with } w^2 = 2Dt;\ \tau, \mu = \text{const.} \tag{5}$$

For time-dependent diffusion coefficients, the differential equation $dw^2/dt = 2D(t)$ applies. This relationship can be rigidly derived from a regular random walking model, which states that the root mean square displacement increases during a time step, dt, by $2D(t)dt$ [19].

To include recombination, we assume that only the remaining fraction, $n_s(t)/n_{s0}$, of the integral sheet charge

carrier concentration, $n_s = \int n(x)dx$, can further diffuse and contribute to an increase of $\sqrt{\langle x^2(t)\rangle}$, which is reflected by Eq. (6). With these definitions, w represents the root mean square displacement of the remaining carrier concentration, and $\sqrt{\langle x^2\rangle}$ is the root mean square displacement of all charge carriers, both recombined and remaining:

$$\frac{d\langle x^2(t)\rangle}{dt} = \frac{n_s(t)}{n_{s0}} 2D(t). \tag{6}$$

The quantity that is experimentally accessible by TRMC and OPTP is the sheet photoconductivity transient, $\Delta\sigma_\Sigma(t)$, which contains the sum of the contributions from photogenerated electrons and holes. The consequences of this superposition of both carrier kinds is discussed later. For now, the sheet photoconductivity, $\Delta\sigma_s(t)$, of a single carrier species is regarded. Additionally, the initial sheet charge carrier concentration, Δn_{s0}, that is photogenerated by each laser pulse can be determined from the excitation conditions. Using the Einstein relationship, $D(t) = \mu(t)k_BT/e$, and the definition of the sheet photoconductivity, $\Delta\sigma_s(t) = e\Delta n_s(t)\mu(t)$, Eq. (7) is derived by direct integration of Eq. (6). This yields the temporal evolution of the root mean square displacement, $\sqrt{\langle x^2(t)\rangle}$, of photogenerated charge carriers from a measured photoconductivity transient:

$$\sqrt{\langle x^2(t)\rangle} = \sqrt{\int_0^t 2\frac{\Delta\sigma_s(t')}{\Delta n_{s0}}\frac{k_BT}{e^2}dt' + \langle x^2(t=0)\rangle}. \tag{7}$$

The mean absolute displacement can be expressed by $\langle|x(t)|\rangle = a\sqrt{\langle x^2(t)\rangle}$. The factor a depends on the spatial distributions of the remaining carriers, $n(x,t)$, and of the recombined carriers, $n_r(x,t)$. For a Gaussian distribution, which usually describes the remaining carriers, a factor $a = \sqrt{2/\pi}$ is gained by solving Eq. (4) in Note 1 within the Supplemental Material [66]. For an exponential distribution, which usually describes the recombined charge carriers, a factor $a = \sqrt{1/2}$ is obtained. We suspect, without rigid proof, that a lies, in general, between $\sqrt{1/2} \le a \le \sqrt{2/\pi}$, which is confirmed for some cases below. This consideration results in the final expression for the mean displacement [Eq. (8)]:

$$\langle|x(t)|\rangle = a(t)\sqrt{\int_0^t 2\frac{\Delta\sigma_s(t')}{\Delta n_{s0}}\frac{k_BT}{e^2}dt'}. \tag{8}$$

As stated earlier, the mean displacement converges to the diffusion length for long times, $L_D = \langle|x(t\to\infty)|\rangle$, which yields

$$L_D = a\sqrt{\int_0^\infty 2\frac{\Delta\sigma_s(t')}{\Delta n_{s0}}\frac{k_BT}{e^2}dt'}, \quad \text{with } \sqrt{1/2} \le a \le \sqrt{2/\pi}. \tag{9}$$

This expression calculates the diffusion length from any (measured) photoconductivity transient, which is verified in the following for several test cases. To this end, it is compared to the precise numerical modeling based on Eqs. (1)–(4), which yields the evolution of the carrier distribution [Figs. 1(a)–1(c)], the photoconductivity transients [Figs. 1(d)–1(f)], and the mean absolute displacements that converge to the diffusion lengths [Figs. 1(g)–1(i)]. The precise numeric solution falls between the prediction of Eqs. (8) and (9) with $\sqrt{1/2} \le a \le \sqrt{2/\pi}$, which confirms the validity of these equations.

Case 1 considers an exponentially decaying mobility with a decay time, τ_μ, of 10 ns [Fig. 1(d)] and an infinite lifetime. Hence, the sheet carrier concentration is constant, and the decay in photoconductivity is exclusively caused by the decrease in mobility [Fig. 1(d)]. Under such conditions, the numerically calculated mean displacement can be reproduced from the photoconductivity transient using the analytical expression [Eqs. (7) and (8)] for a factor $a = \sqrt{2/\pi}$ [Fig. 1(g)]. This factor is expected since the distribution profile always remains Gaussian. At sufficiently long times, it converges to a diffusion length of $L_D = \sqrt{4D\tau_\mu/\pi}$, which is obtained by analytically solving Eq. (9).

Case 2 assumes a constant mobility and a carrier concentration that decays exponentially with a constant lifetime, τ, of 10 ns. Hence, the photoconductivity decays as in case 1 but is due to carrier recombination instead. Again, the mean displacement can initially be described with the prefactor $a = \sqrt{2/\pi}$. However, for times longer than the average lifetime, it converges to a diffusion length that contains the prefactor $a = \sqrt{1/2}$. The reason for this changing prefactor is the exponential distribution of recombined carriers, for which $a = \sqrt{1/2}$ applies, becoming more dominant than the Gaussian distribution of the remaining carriers, for which $a = \sqrt{2/\pi}$ applies [Fig. 1(b)]. Solving Eq. (9) analytically for the final exponential distribution of recombined carriers yields the classical equation of the diffusion length: $L_D = \sqrt{D\tau}$.

Case 3 models an initial decay of the mobility from 1 to 0.1 $\mathrm{cm^2\,V^{-1}\,s^{-1}}$ with a decay time of 100 ps and subsequent recombination with a lifetime of 10 ns, which may be considered as a rough representation of trapping and recombination in a metal oxide. The mean displacement is described initially by the a factor, $\sqrt{2/\pi}$, and then converges to a diffusion length with an intermediate factor, $\sqrt{1/2} \le a \le \sqrt{2/\pi}$.

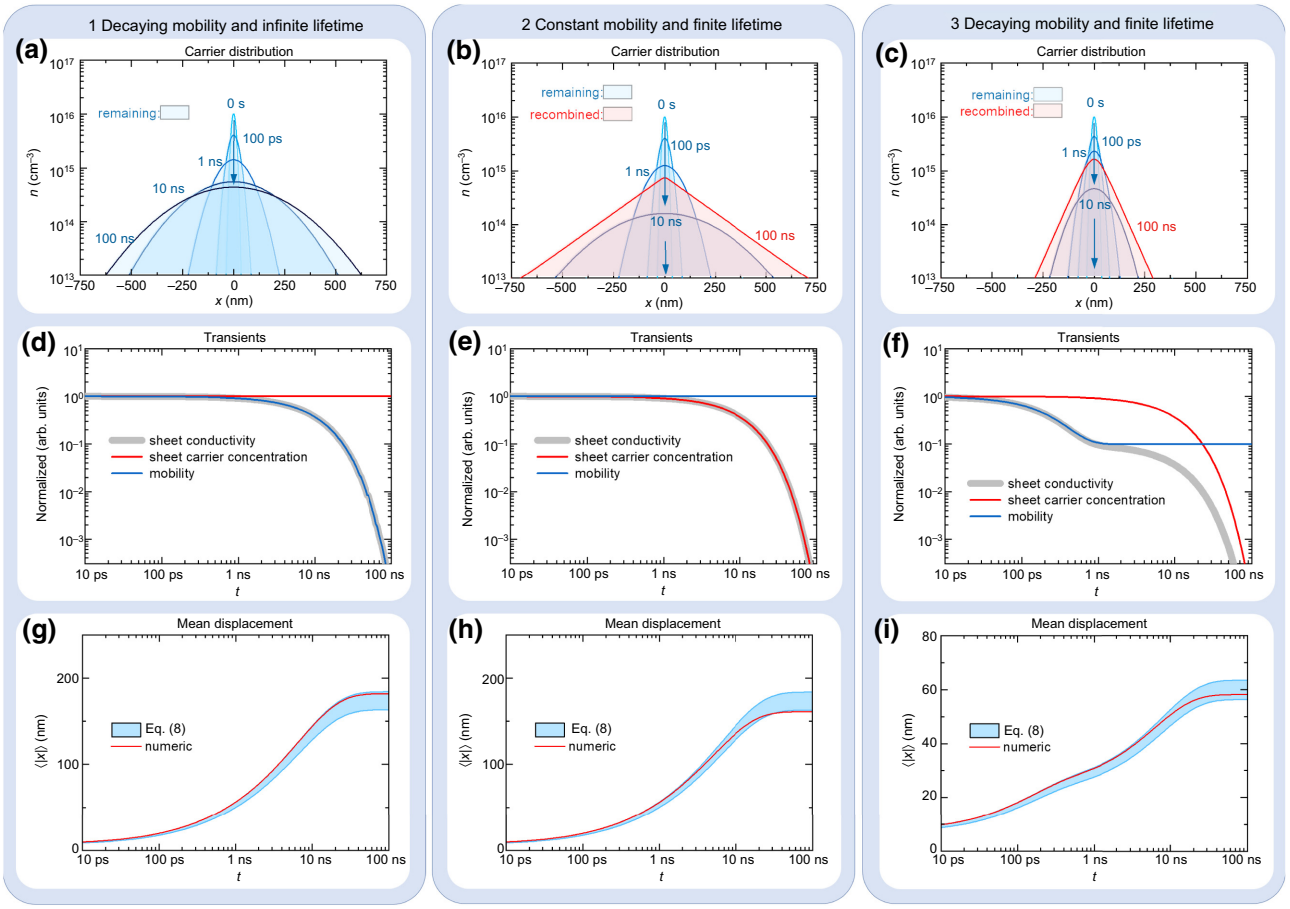

FIG. 1. Confirming the generalized diffusion length by numerical modeling. (a)–(c) Evolution of Gaussian carrier distributions modeled numerically with Eq. (1) for (a) mobility decaying with a decay time, τ_μ, of 10 ns from an initial value of 1 cm^2 V^{-1} s^{-1}; (b) constant mobility of 1 cm^2 V^{-1} s^{-1} and a lifetime, τ, of 10 ns; and (c) mobility decaying with a decay time of 100 ps from an initial value of 1 cm^2 V^{-1} s^{-1} and a lifetime of 10 ns. Final distribution of the recombined carriers is estimated at $t = 100$ ns, $\gg\tau$, and is shown in red. (d)–(f) Normalized transients of the mobility (blue line), sheet carrier concentration (red line), and sheet conductivity (thick gray line). (g)–(i) Evolution of the mean absolute displacement. Precise numerical value (red line) is, in general, between the values of analytical Eq. (8) with the factor $\sqrt{1/2} < a < \sqrt{2/\pi}$. For decaying mobility and without recombination (case 1), $a = \sqrt{2/\pi}$. For constant mobilities and recombination (case 2), it converges to a diffusion length with a factor $a = \sqrt{1/2}$.

In the next section, this analysis is applied to experimentally obtained OPTP and TRMC transients. In such cases, it is often unknown which factor a applies, since mobility and concentrations may decay simultaneously. Hence, we recommend using the mean value of 0.75. The difference between the minimum $\left(\sqrt{1/2}\right)$ and maximum $\left(\sqrt{2/\pi}\right)$ values of ±6% is relatively small and can be included in the error bar. However, this error is small compared to the accuracy of ±25% of our OPTP- and TRMC-derived mobilities (and diffusion lengths), which is estimated from a recent comparison with 15 other OPTP and TRMC laboratories [20].

A general limitation of TRMC and OPTP is that the obtained photoconductivity contains the sum of electron and hole contributions, which cannot be distinguished here. Applying Eq. (8) to such photoconductivity yields a combined (not the sum) diffusion length of both carrier species. Strictly, Eq. (8) should be multiplied by a factor, $b_e = \sqrt{\mu_e/(\mu_e + \mu_h)}$, to obtain exclusively the electron diffusion length (analogous for the hole diffusion length) [21]. However, as the individual mobilities (μ_e, μ_h) are usually not known, we assume here equal electron and hole mobilities, resulting in $b_e = b_h = \sqrt{1/2}$. Using this b factor and the mean value of the a factor leads to Eq. (10), which estimates the diffusion length directly from a photoconductivity transient, $\Delta\sigma_\Sigma(t)$, that is measured by OPTP or TRMC. The corresponding temporal evolution of the mean absolute displacement is described by Eq. (10), after replacing the upper limit of the integral (∞) by the time t:

$$L_D \approx 0.75\sqrt{\int_0^\infty \frac{\Delta\sigma_\Sigma(t)}{\Delta n_{s0}}\frac{k_B T}{e^2}dt}. \tag{10}$$

Despite the mentioned uncertainties, the obtained (approximate) diffusion length can be used as a figure of merit for the diffusion of charge carriers, which allows a comparison between different materials from the (OPTP- and TRMC-derived) photoconductivity transients without the challenge of a clear assignment of the underlying relaxation processes and without distinguishing electron and hole contributions.

III. CARRIER DIFFUSION IN $BiVO_4$

First, the generalized analysis of the diffusion length [Eq. (10)] is applied to TRMC- and OPTP-derived photoconductivity transients that are measured for *n*-type $BiVO_4$. All method (OPTP [22–29], TRMC [30–33]) and sample details [34] are found in Notes 3 and 5 within the Supplemental Material [66], respectively.

A. Joint photoconductivity transients

Figures 2(a)–2(c) show the TRMC and OPTP transients, as commonly reported and analyzed by the different research communities. The OPTP community usually reports sheet photoconductivity transients ($\Delta\sigma_\Sigma$). As displayed in Fig. 2(a), the transients are often divided by the initially photogenerated sheet charge carrier concentration, Δn_0, and the elementary charge, e, to determine the charge carrier mobility from the initial amplitude in units of $cm^2\,V^{-1}\,s^{-1}$. However, the transient still represents the sheet photoconductivity transient and is not necessarily a mobility decay.

The TRMC community usually prefers to state the photoconductance, ΔG, which is the sheet photoconductivity, $\Delta\sigma_\Sigma$, scaled by the dimensions of the sample. However, the transient behavior of $\Delta\sigma_\Sigma$ and ΔG is the same. The photoconductivity transients measured by ST-TRMC and

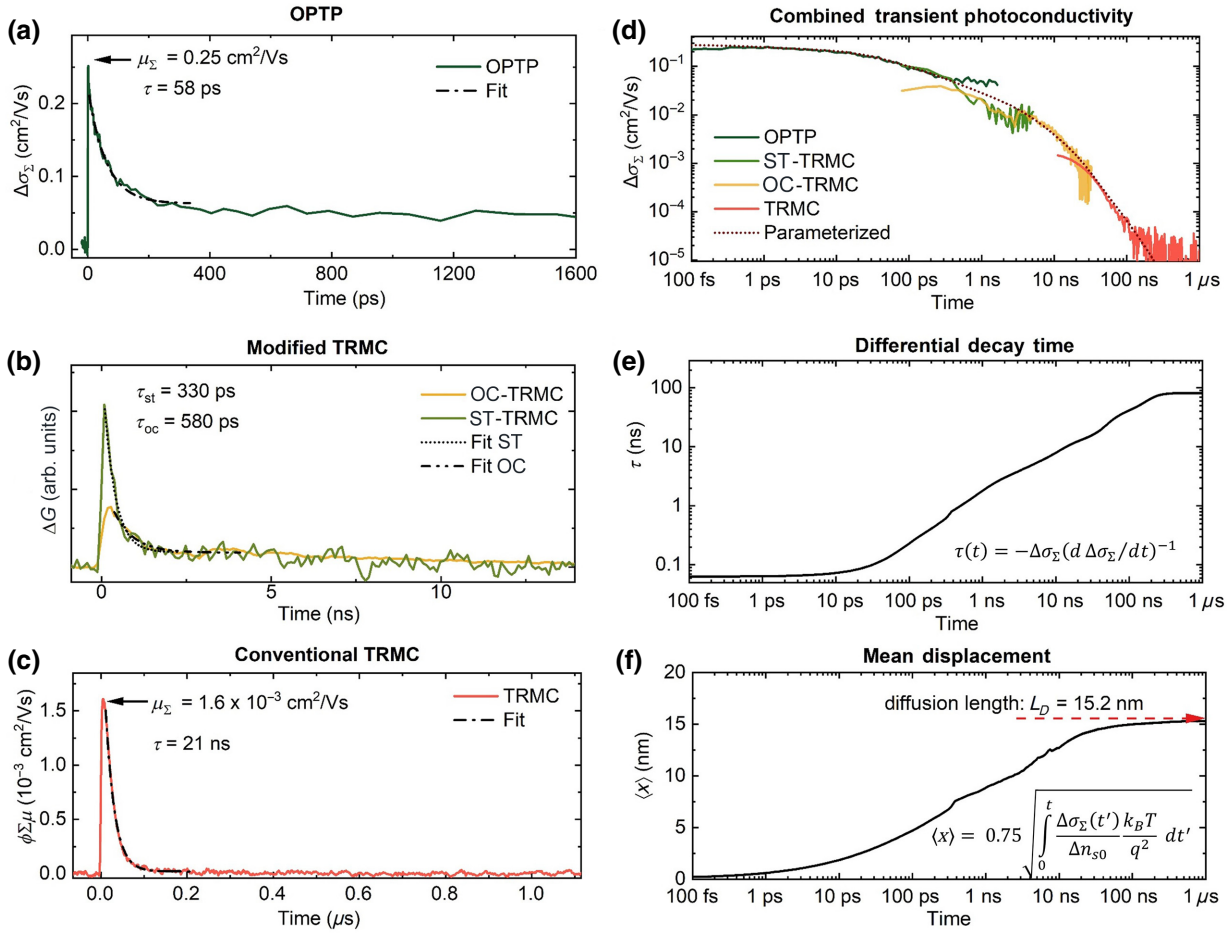

FIG. 2. Diffusion and recombination of photogenerated charge carriers in $BiVO_4$. Photoconductivity transients of a PLD-deposited $BiVO_4$ thin film on fused silica are measured by (a) OPTP, (b) ST- and OC-TRMC, and (c) TRMC. Mobilities, μ_Σ, and decay times, τ, of the individual techniques are obtained from the initial amplitudes and from modeling the initial decays with $\exp(-t/\tau)$, respectively. (d) Superimposed measured photoconductivity transients, $\Delta\sigma_\Sigma(t)$, and a parameterized joint transient as a guide for the eye. (e) Temporal evolution of the decay time, $\tau(t)$, obtained from the parameterized joint transient. (f) Temporal evolution of the mean absolute displacement, $\langle x\rangle(t)$, of photogenerated charge carriers in $BiVO_4$ obtained from the OPTP- and TRMC-derived photoconductivity transients by Eq. (10). Value approaches a diffusion length of about 15 nm at sufficiently long times (>100 ns).

OC-TRMC are shown in Fig. 2(b). The absolute mobilities cannot be calculated since the sensitivity factors of these TRMC configurations are not well defined.

For conventional TRMC in a closed cavity [Fig. 2(c)], the photoconductance is usually translated into units of $cm^2\,V^{-1}\,s^{-1}$ analogous to the OPTP analysis. The commonly used label is $\phi\Sigma\mu$, which represents that the mobility is given by the product of the free carrier quantum yield, ϕ, and the sum of the electron mobility and hole mobility.

The TRMC-derived peak mobility of $BiVO_4$ in this work is roughly a factor of about 100 smaller than earlier TRMC reports from our group on $BiVO_4$ [35, 36]. Recently, we observe a similar discrepancy for $\alpha - SnWO_4$[32] and identified, in combination with different illumination intensities and different sample preparations, a previously incorrect determination of the sensitivity factor, K, of the cavity as the main origin [12,37], which occurs also in studies on other metal oxides (e.g., Refs. [38,39]). The correct determination of K and further experimental details are described in Notes 2–4 within the Supplemental Material [66]).

The OPTP transient and the TRMC transients of $BiVO_4$ have different initial mobilities and different initial decay times [$\sim\exp(-t/\tau)$], i.e., 60 ps and 0.25 $cm^2\,V^{-1}\,s^{-1}$ for OPTP, 330 ps for ST-TRMC, 550 ps for OC-TRMC, and 24 ns and 0.0016 $cm^2\,V^{-1}\,s^{-1}$ for TRMC. These decay times are similar to those previously reported for $BiVO_4$ with the individual techniques [35,36]. Hence, it is not clear which of these values are the relevant ones for characterizing carrier transport and recombination in the material, e.g., in terms of determining a diffusion length. In Fig. 2(d), the individual OPTP and TRMC transients are combined to resolve this contradiction. Since ST- and OC-TRMC transients are obtained in arbitrary units, they are scaled to overlap with the TRMC and OPTP transients. These modified TRMC setups allow the gap in the time window between the OPTP (<2 ns) and conventional TRMC (>10 ns) transients to be bridged. To reduce the noise level, a joint parameterized photoconductivity transient is generated (dotted curve), which spans over 7 orders of magnitude from 0.1 ps to 1 μs. The stitching and parameterization process is described in the methods section within the Supplemental Material [66]. The combined transients shown in Fig. 2(d) match reasonably well, except for the region around 1 ns. Here, the long component of the OPTP transient deviates from the combined transient. This OPTP signal at longer times (>300 ps) was previously attributed to a phonon or polaron feature in $BiVO_4$ at 1.8 THz [29] and could be seen at about 1.8 THz in the frequency-resolved terahertz mobility spectrum in Fig. S4(b) within the Supplemental Material [66]. Hence, this long component does not reflect purely electronic transport and should be disregarded here. Additionally, a small shoulder can be observed at about 3 ns in the OC- or ST-TRMC transient, which can be attributed to reflections within the measurement electronics and is, therefore, a measurement artifact.

The combined transient shows that the difference between the TRMC-derived and OPTP-derived mobilities is a consequence of the photoconductivity decay within the time resolution of the conventional TRMC of about 10 ns. However, the interpretation of this decay is not trivial.

A possible interpretation would be that the photoconductivity decay is caused by charge carrier recombination and the corresponding decay of the carrier concentration. In this case, TRMC yields an underestimated mobility value due to its limited time resolution, and the OPTP-derived mobility will be the more relevant one.

An alternative interpretation is that the average mobility of the charge carriers decays due to their relaxation from mobile band states into localized defects and polaronic or excitonic states. In such a case, the TRMC mobility likely reflects the effective mobility after relaxation and may yield the relevant value for the operation of the photoelectrode in a steady state. Previous Seebeck measurements of Mo-doped and W-doped $BiVO_4$ reveal electron mobilities of about 10^{-4} $cm^2\,V^{-1}\,s^{-1}$, which supports this second interpretation [29].

Still, the distinction between mobility decay and charge carrier recombination remains somewhat unclear. This challenge also leads to an ambiguous interpretation of the decay times. Figure 2(e) shows that the differential lifetime, $\tau(t) = -\sigma_\Sigma(d\sigma_\Sigma/dt)^{-1}$, determined from the parameterized combined conductivity transient, continuously increases over time. It is therefore unclear which of these decay times represent a charge carrier lifetime or a decay time of the charge carrier mobility.

B. The diffusion length

To overcome these issues, we implement the generalized analysis for the diffusion length and the time-dependent displacement that is derived in the previous section. This analysis does not require any *a priori* distinction between the decay in mobility and the decay due to recombination. The evolution of the mean displacement of photogenerated charge carriers in the $BiVO_4$ thin film, grown by pulsed laser deposition (PLD) is shown in in Fig. 2(f). It is calculated from the combined OPTP, TRMC, OC-TRMC, and ST-TRMC photoconductivity transients [Fig. 2(d)] using Eqs. (7) and (8). Notably, in contrast to the differential decay time, this mean displacement is obtained directly from the measured transients without parameterization or smoothing. The mean displacement in Fig. 2(f) shows that the charge carriers in PLD-deposited $BiVO_4$ diffuse about 8 nm within the first nanosecond, which is roughly the time window of the OPTP setup. Beyond 1 ns, diffusion slows down and converges to a diffusion length of roughly 15 nm.

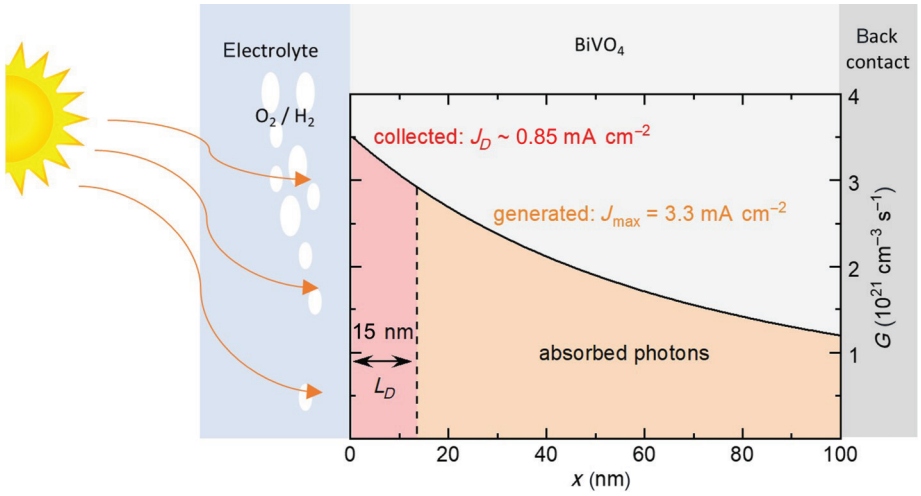

FIG. 3. Rough estimation of photocurrent collection by diffusion. Modeled profile of charge carrier generation, G, in a $BiVO_4$ thin film based on its absorption coefficient and the AM1.5G sun spectrum. Total absorbed sunlight generates a photocurrent $J_{max} = q \int G dx$. Photocurrent collected by diffusion, J_D, is estimated by the carriers that are generated within the diffusion length L_D.

C. Comparison to charge transport in a photoelectrode

To determine whether a material can serve as a good photoabsorber in a solar energy conversion device, the diffusion length is often compared to the layer thickness (or the absorption depth). In this case, the thickness of the investigated PLD $BiVO_4$ film is 100 nm, which is much larger than the determined diffusion length. Hence, these films are unlikely to show high photon-to-current conversion efficiencies.

If one carrier type limits charge extraction from the photoabsorber, the short-circuit photocurrent, J_{sc}, can be estimated roughly by the fraction of photons that are absorbed within a distance L_D from the interface that extracts the limiting carrier kind, as shown in Fig. 3. Interestingly, for $BiVO_4$, electron transport is reported to limit the extraction of photogenerated carriers, although electrons are the majority carrier type [40]. The absorption coefficient of $BiVO_4$ and the AM1.5G solar spectrum are shown in Figs. S2(a) and S2(b) within the Supplemental Material [66] and 10% reflection losses are assumed. For a thickness of 100 nm, a maximum current of 3.3 mA cm^{-2} can be extracted, as shown in Fig. S2(b) within the Supplemental Material [66]. However, within the diffusion length of 15 nm, only about 0.85 mA cm^{-2} are collected if the relevant interface is at the same side as the illumination.

Despite the expected low electric currents discussed above, our previous PLD $BiVO_4$ photoanodes—prepared with the same procedure as the sample in this study (but on fluorine-doped tin oxide)—demonstrated AM1.5 photocurrents of 2.4 mA cm^{-2} at 1.23 V versus the reversible hydrogen electrode [34]. This large photocurrent cannot be explained by the diffusion length of only 15 nm and is instead in line with a larger collection length of at least 50 nm. Therefore, it is attributed to drift transport within the built-in space-charge regions as well as to the application of a bias potential. Nevertheless, long diffusion lengths usually correlate with long drift lengths, as both are a function of carrier mobility and lifetime [1]. Hence, the diffusion length remains an important figure of merit in predicting high-efficiency materials.

To relate our results on a particular PLD-grown thin film to the potential of $BiVO_4$ in general, several considerations should be noted. First, several studies have observed anisotropic transport and trap filling in $BiVO_4$ [35,41,42]. Thus, oriented films, as shown in Ref. [43], exhibit higher mobilities, longer diffusion lengths, and, therefore, higher photocurrents than the polycrystalline $BiVO_4$ with randomly oriented grains investigated here. Furthermore, the OPTP and TRMC transients in this work are measured at an incident photon flux of about 3×10^{13} cm^{-2} per pulse. This intensity generates a charge carrier concentration that is orders of magnitude larger than the one generated under continuous solar illumination [44]. Since mobility and lifetime often depend on the generated carrier concentration, for example, due to trap filling or higher-order recombination [44], the diffusion length reported here may differ from that under 1-sun conditions.

IV. MULTIPLE TRAPPING IN *a*-Si : H

To investigate how general the presented approach is, we also investigate *a*-Si : H, a material well known to have complex charge carrier dynamics. Mobilities and lifetimes are time dependent, as photogenerated carriers trap over time in ever deeper and more localized states; this is called multiple trapping [45].

The measured photoconductivity transients of *a*-Si : H, prepared by a plasma-enhanced chemical vapor deposition

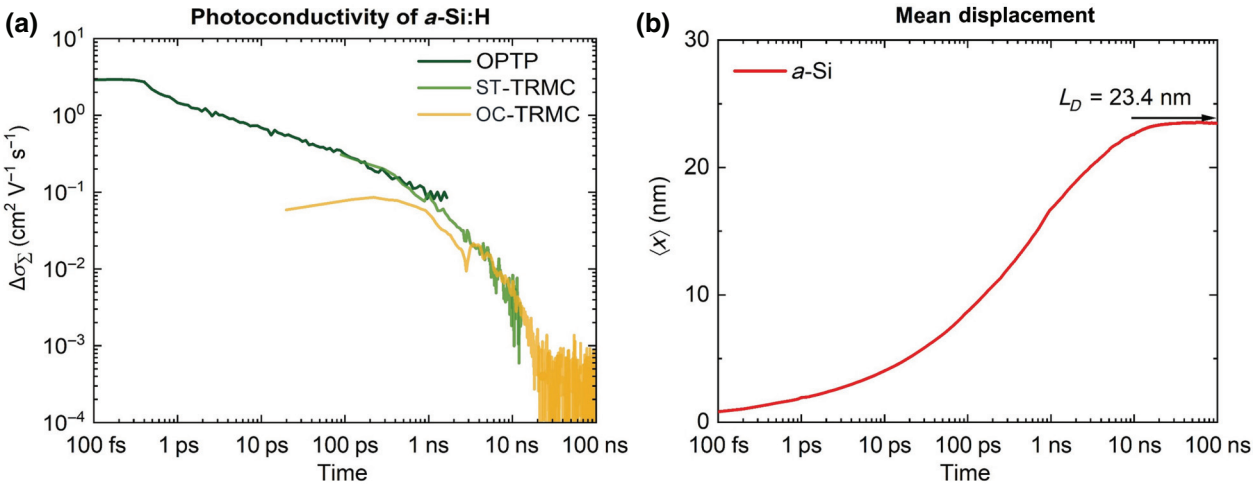

FIG. 4. Charge carrier diffusion and recombination in a-Si. (a) Photoconductivity transients measured by OPTP, OC-TRMC, and ST-TRMC. (b) Temporal evolution of the mean displacement of photogenerated charge carriers obtained by Eq. (10) converges to a diffusion length L_D.

process, according to Ref. [46], are shown in Fig. 4(a). The OPTP-derived sum of electron mobility and hole mobility of 2.9 $cm^2 V^{-1} s^{-1}$ is in line with a previous OPTP study on *a*-Si, which reported 2 $cm^2 V^{-1} s^{-1}$ [47]. These values for the sum of electron mobility and hole mobility are in the range of electron mobilities of about 1–10 $cm^2 V^{-1} s^{-1}$ previously reported from Hall and conductivity or time-of-flight measurements for transport in extended states of *a*-Si [48,49]. However, carrier localization in band tails is reported to reduce the effective electron mobilities from the extended state mobilities to about 0.1 $cm^2 V^{-1} s^{-1}$ [48–50]. These lower mobilities are reported under continuous illumination and, therefore, represent a relaxed quasiequilibrium. In contrast, OPTP resolves the carrier mobilities in the extended states before the carriers relax into the band tails. Additionally, localized tail states are mostly filled during the OPTP (and TRMC) measurements by the relatively large photogenerated carrier concentrations of about 10^{18} cm^{-3}. Similar filling of defect states can be expected for measurements on metal oxides and is reported to increase the TRMC-derived mobilities in $BiVO_4$ [35].

The OPTP photoconductivity transients of *a*-Si : H are combined in Fig. 4(a) with the ST- or OC-TRMC transients. The TRMC transient is significantly smeared out by the TRMC time resolution of about 10 ns at the times the OC-TRMC vanishes in the noise floor. Therefore, it does not overlap with the other transients (Fig. S3 within the Supplemental Material [66]) and is omitted here. Although previous TRMC studies on *a*-Si : H showed significant sample-to-sample variations [51] and a dependence of the photoconductivity decay on annealing temperature [52] and sample composition [53], they obtained, in general, longer transients with slower decays. Hence, the sample studied here seems to be of rather poor quality.

Based on the combined photoconductivity transients measured here, the mean displacement can be obtained by our generalized analysis and is shown in Fig. 4(b). It converges after about 10 ns to a finite diffusion length of 23 nm. Again, this value is rather low compared to previous reports on high-performance *a*-Si : H with diffusion lengths of up to several hundred nanometers and is likely connected to the rather fast TRMC decay compared to previous studies. Note that the *a*-Si : H thin-film studied here is stored for about seven years under ambient conditions, which possibly causes oxidation and a loss of H passivation, explaining the relatively low diffusion length and fast decay. A similar low diffusion length of about 10 nm was previously reported for films with high oxygen contamination [54]. Nevertheless, despite the obtained diffusion length not being representative of state-of-the-art *a*-Si : H, our results demonstrate the applicability of our method for complex semiconductors.

V. GENERAL APPLICABILITY

Until now, our generalized approach has been tested on two rather complex systems. For a thorough comparison with reference data and the conventional analysis, the photoconductivity transients of a single crystalline silicon wafer (*c*-Si) and a triple-cation lead halide perovskite thin film on fused silica substrate are measured and shown in Fig. 5(a). These transients are rather simple, as the photoconductivities are approximately constant in the time windows of the OPTP and OC- or ST-TRMC measurements and decay in the time window of the conventional TRMC. Figure 5(b) reveals that the decay for *c*-Si is approximately single exponential and can be described by a charge carrier lifetime of 322 μs. The initial sum mobility is 1930 $cm^2 V^{-1} s^{-1}$. Assuming equal electron

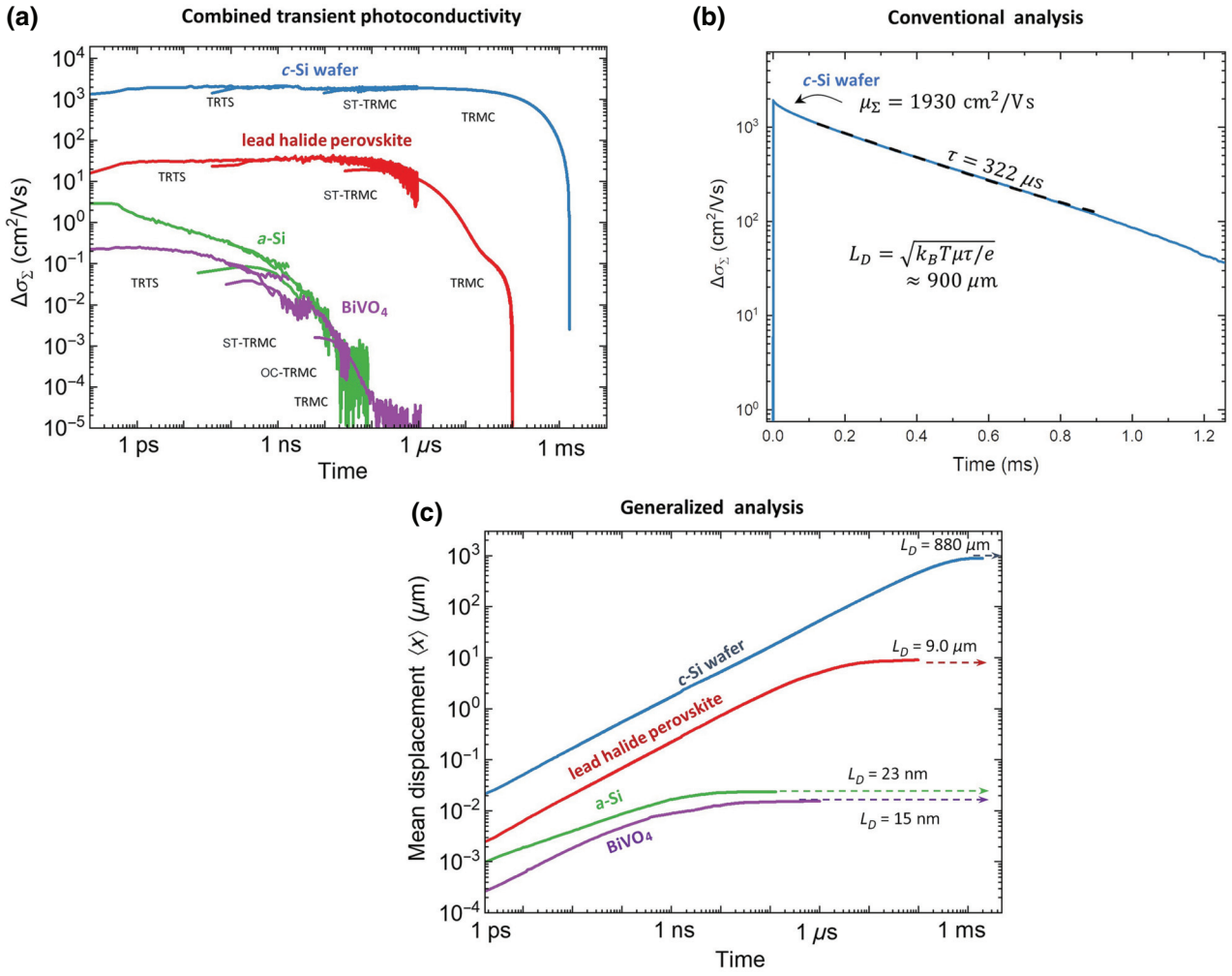

FIG. 5. Application and validation for simple well-known materials. (a) Photoconductivity transients of a single-crystalline silicon wafer, a lead halide perovskite thin film, as well as a-Si and $BiVO_4$ measured by OPTP, ST- or OC-TRMC, and conventional TRMC. (b) Transient of c-Si appears approximately monoexponential with a fitted lifetime of 322 μs, and the mobility is taken from the initial amplitude. Conventional analysis of the diffusion length yields 900 μm. (c) Temporal evolution of the mean displacements of photogenerated charge carriers obtained by Eq. (10). They converge to finite diffusion lengths that are in line with conventional analysis.

and hole mobilities, a diffusion length of about 900 μm can be calculated by the conventional approach, $L_D = \sqrt{\mu\tau k_B T/q}$.

In comparison, our generalized analysis by Eq. (10) is shown in Fig. 5(c) and yields mean displacements that converge to diffusion lengths of 880 μm for c-Si and 9.0 μm for the halide perovskite. This diffusion length for c-Si is in excellent agreement with the conventional approach [Fig. 5(c)] and, for all four materials, the obtained diffusion length is in line with literature values obtained by other approaches, as shown in Table S2 within the Supplemental Material [55–62,66,67].

Finally, some limitations of the presented approach should be mentioned. A practical challenge encountered here is the bandwidth of the detection electronics of the TRMC setup. Especially for very long signals, as observed for c-Si, the photoconductivity transients are initially obscured for times beyond 70 μs due to the limited bandwidth of the amplifier (see Fig. S12 within the Supplemental Material [66]). Hence, the integral in Eq. (10) should only be performed up to a time that is still within the bandwidth of the TRMC setup. As the mean displacement initially does not converge to a finite diffusion length within the first 70 μs, the TRMC detector amplifier has to be modified to achieve a lower frequency cutoff.

A cause of experimental variation is the injection dependence, which can be seen in Fig. S13 within the Supplemental Material [66] for the TRMC transients of the perovskite sample. Thus, the value of the diffusion length will vary accordingly. These variations for perovskites are a consequence of second-order (radiative) recombination, which becomes stronger at higher injection [20,62].

A more fundamental limitation of the presented approach is that it does not consider potential frequency dependence of the charge mobilities, as the TRMC, OC- or ST-TRMC, and OPTP probe transport at different frequencies of 9 GHz, 30 GHz, and 1 THz, respectively. For the probed materials such a frequency dependence is rather small, as shown in Figs. S3–S5 within the Supplemental Material [66]. For example, the *c*-Si sample exhibits free-carrier transport and a Drude-like spectrum with a dc sum mobility of 1930 $cm^2\,V^{-1}\,s^{-1}$ that stays constant up to about 100 GHz and then decreases to about 1000 cm^2/Vs at THz frequencies. For long-range diffusion of free carriers, as in *c*-Si, the modeled dc mobility should be used as the initial amplitude of the photoconductivity transient when calculating the diffusion length.

However, carrier confinement can lead to strong differences between mobilities at THz and GHz frequencies and differences between long-range and short-range transport [63–65]. It can result in an offset between TRMC-, OC- or ST-TRMC-, and OPTP-derived transients and mobilities. Under these circumstances, it is not straightforward to combine these TRMC and OPTP transients and to calculate the diffusion length from Eq. (10). However, also the classical calculation of the diffusion length, $L_D = \sqrt{\mu\tau k_B T/q}$, is ambiguous in this case, and it is not a particular issue of our generalized approach. It leads to the question, at which frequency should the mobility be measured to predict carrier diffusion at which length scales? These issues will be addressed in a future publication that we are currently preparing. For the materials shown in this work, the TRMC and OPTP transients can overlap without significant offset, which implies that carrier confinement on the nanometer length scale is not relevant.

VI. CONCLUSIONS

A simple analytical equation is presented that can be used to calculate the diffusion length of photogenerated charge carriers directly from photoconductivity transients. Hence, the presented method does not require making a (often ambiguous) distinction between a decay in mobility (due to trapping, polaron formation, etc.) and a decay in carrier concentration (recombination). Furthermore, in contrast to conventional analyses, this approach also accommodates time-dependent charge carrier lifetimes and mobilities, which are often exhibited by disordered materials and metal oxides. The presented analysis is validated by comparison with numerical diffusion-recombination simulations. Our analysis shows that the same photoconductivity decay caused by recombination or a decaying mobility results in comparable diffusion lengths that differ only by a factor of $2/\sqrt{\pi}$. Hence, the often-puzzling origin of photoconductivity decays results only in a minor uncertainty of $\pm 6\%$ for the obtained diffusion length.

Our generalized approach is applied to combined TRMC and OPTP transients to monitor the diffusion of photogenerated charge carriers in PLD-grown $BiVO_4$ and *a*-Si : H from 100 fs up to 1 μs. For $BiVO_4$, TRMC- and OPTP-derived photoconductivity transients can be combined consistently with respect to both decay kinetics and amplitudes and yield a finite diffusion length of about 15 nm. Such a diffusion length is too small for an efficient photoabsorber and explains the inferior performance compared to Si-based photoelectrodes. To achieve sufficient carrier collection in $BiVO_4$, drift transport provided by a built-in or applied electric field is required. However, when relating the obtained diffusion lengths to the performance of a solar cell or a PEC cell, care must be taken due to the unknown relative contributions of photogenerated electrons and photogenerated holes to the photoconductivity signal, and due to the higher injection levels during the OPTP and TRMC measurements compared to 1-sun continuous illumination. Still, the obtained diffusion length is a figure of merit that can guide the future development of energy conversion materials.

The presented approach is simpler, more robust, and can be applied to a wider range of materials than the conventional analysis. It is simpler because it does not require a fitting of the photoconductivity transient but simply integrates it. It is more robust, as fitting depends on the starting conditions, parameter boundaries, and the decay model used, which are obsolete in our case, and make it particularly suited for automated analysis of large data sets. The wide applicability is demonstrated here on diverse material classes of *a*-Si : H thin film, a single crystalline silicon wafer, and a hybrid lead halide perovskite thin film. However, for materials with strongly frequency-dependent mobilities, such as those induced by carrier confinement, it cannot be applied straightforwardly. In contrast, it is observed here that, even for *a*-Si, the GHz and THz mobilities are comparable, and the method is applicable to disordered materials and can resolve the initial mobility of free carriers before they are trapped.

ACKNOWLEDGMENTS

We kindly thank Bernd Stannowski from HZB for the preparation of the *a*-Si : H sample. We further thank Ibbi Ahmet for proofreading the manuscript and for fruitful discussions. We also would like to thank Elias Hartung and Orestis Karalis for supporting the TRMC and UV-vis measurements on *c*-Si and the perovskite. The authors acknowledge financial support for this work from the Helmholtz International Research School "Hybrid Integrated Systems for Conversion of Solar Energy" (HI-SCORE), an initiative cofunded by the Initiative and Networking Fund of the Helmholtz Association (Grant No. HIRS-008).

M.K., M.Sc., and H.H. initiated and outlined the study. M.Sc. performed and analyzed the TRMC, OC-TRMC, ST- TRMC and OPTP measurements. M.Sc. and H.H. wrote the manuscript and designed the figures. H.H. derived the equations and performed the numeric modeling. H.H. and D.F. supervised the project. R.E. and D.F modified the TRMC, OC-TRMC, and ST-TRMC setups and supervised these measurements. K.S. established the impedance model fitting routine. R.v.d.K. supervised the contributions from his group. M.K. prepared the $BiVO_4$ sample. M.St. prepared the halide perovskite sample. All authors discussed the results and revised the manuscript.

[1] T. Kirchartz, J. Bisquert, I. Mora-Sero, and G. Garcia-Belmonte, Classification of solar cells according to mechanisms of charge separation and charge collection, Phys. Chem. Chem. Phys. **17**, 4007 (2015).

[2] T. Kirchartz and U. Rau, What makes a good solar cell?, Adv. Energy Mater. **8**, 1703385 (2018).

[3] P. Kaienburg, L. Krückemeier, D. Lübke, J. Nelson, U. Rau, and T. Kirchartz, How solar cell efficiency is governed by the $A\mu\tau$ product, Phys. Rev. Res. **2**, 023109 (2020).

[4] T. J. Savenije, A. J. Ferguson, N. Kopidakis, and G. Rumbles, Revealing the dynamics of charge carriers in polymer:fullerene blends using photoinduced time-resolved microwave conductivity, J. Phys. Chem. C **117**, 24085 (2013).

[5] M. Kunst and G. Beck, The study of charge carrier kinetics in semiconductors by microwave conductivity measurements, J. Appl. Phys. **60**, 3558 (1986).

[6] U. T. Tayvah, J. Neu, J. A. Spies, C. A. Schmuttenmaer, and G. W. Brudvig, Ultrafast terahertz spectroscopy provides insight into charge transfer efficiency and dynamics in artificial photosynthesis, Photosynth. Res. **151**, 145 (2022).

[7] J. A. Spies, J. Neu, U. T. Tayvah, M. D. Capobianco, B. Pattengale, S. Ostresh, and C. A. Schmuttenmaer, Terahertz spectroscopy of emerging materials, J. Phys. Chem. C **124**, 22335 (2020).

[8] C. Lohaus, A. Klein, and W. Jaegermann, Limitation of Fermi level shifts by polaron defect states in hematite photoelectrodes, Nat. Commun. **9**, 4309 (2018).

[9] A. J. E. Rettie, W. D. Chemelewski, D. Emin, and C. B. Mullins, Unravelling small-polaron transport in metal oxide photoelectrodes, J. Phys. Chem. Lett. **7**, 471 (2016).

[10] A. Kay, M. Fiegenbaum-Raz, S. Müller, R. Eichberger, H. Dotan, R. van de Krol, F. F. Abdi, A. Rothschild, D. Friedrich, and D. A. Grave, Effect of doping and excitation wavelength on charge carrier dynamics in hematite by time-resolved microwave and terahertz photoconductivity, Adv. Funct. Mater. **1**, 1901590 (2019).

[11] M. Ziwritsch, S. Müller, H. Hempel, T. Unold, F. F. Abdi, R. Van De Krol, D. Friedrich, R. Eichberger, R. Van De Krol, D. Friedrich, *et al.*, Direct time-resolved observation of carrier trapping and polaron conductivity in $BiVO_4$, ACS Energy Lett. **1**, 888 (2016).

[12] M. Kölbach, H. Hempel, K. Harbauer, M. Schleuning, A. Petsiuk, K. Höflich, V. Deinhart, D. Friedrich, R. Eichberger, F. F. Abdi, *et al.*, Grain boundaries limit the charge carrier transport in pulsed laser deposited $\alpha - SnWO_4$ thin film photoabsorbers, ACS Appl. Energy Mater. **3**, 4320 (2020).

[13] M. H. Cohen, E. N. Economou, and C. M. Soukoulis, Microscopic mobility, Phys. Rev. B **30**, 4493 (1984).

[14] J. Schafferhans, A. Baumann, A. Wagenpfahl, C. Deibel, and V. Dyakonov, Oxygen doping of P3HT:PCBM blends: Influence on trap states, charge carrier mobility and solar cell performance, Org. Electron. **11**, 1693 (2010).

[15] H. Bässler and A. Köhler, in *Charge Transport in Organic Semiconductors BT—Unimolecular and Supramolecular Electronics I: Chemistry and Physics Meet at Metal-Molecule Interfaces*, edited by R. M. Metzger (Springer Berlin Heidelberg, Berlin, Heidelberg, 2012), p. 1.

[16] D. Friedrich, L. Valldecabres, M. Kunst, T. Moehl, S. M. Zakeeruddin, and M. Grätzel, Dye regeneration dynamics by electron donors on mesoscopic TiO_2 films, J. Phys. Chem. C **118**, 3420 (2014).

[17] A. Marchioro, J. Teuscher, D. Friedrich, M. Kunst, R. van de Krol, T. Moehl, M. Grätzel, and J.-E. Moser, Unravelling the mechanism of photoinduced charge transfer processes in lead iodide perovskite solar cells, Nat. Photonics **8**, 250 (2014).

[18] D. Friedrich, L. Valldecabres, and M. Kunst, Charge carrier kinetics in ZnO films and nanorods, Chem. Phys. Lett. **515**, 109 (2011).

[19] B. Fristedt and L. Gray, *A Modern Approach to Probability Theory* (Birkhäuser Boston, Boston, MA, 1997).

[20] H. Hempel, T. J. Savenjie, M. Stolterfoht, J. Neu, M. Failla, V. C. Paingad, P. Kužel, E. J. Heilweil, J. A. Spies, M. Schleuning, *et al.*, Predicting solar cell performance from terahertz and microwave spectroscopy, Adv. Energy Mater. **12**, 2102776 (2022).

[21] N. K. Tailor, Yukta, R. Ranjan, S. Ranjan, T. Sharma, A. Singh, A. Garg, K. S. Nalwa, R. K. Gupta, and S. Satapathi, The effect of dimensionality on the charge carrier mobility of halide perovskites, J. Mater. Chem. A **9**, 21551 (2021).

[22] C. Strothkämper, A. Bartelt, R. Eichberger, C. Kaufmann, and T. Unold, Microscopic mobilities and cooling dynamics of photoexcited carriers in polycrystalline $CuInSe_2$, Phys. Rev. B: Condens. Matter Mater. Phys. **89**, 1 (2014).

[23] H. Hempel, *Investigation of Charge Carrier Dynamics in Novel Photovoltaic Materials* (Freie Univ. Berlin, Berlin, Berlin, 2020).

[24] H. Hempel, T. Unold, and R. Eichberger, Measurement of charge carrier mobilities in thin films on metal substrates by reflection time resolved terahertz spectroscopy, Opt. Express **25**, 17227 (2017).

[25] D. A. Grave, D. S. Ellis, Y. Piekner, M. Kölbach, H. Dotan, A. Kay, P. Schnell, R. van de Krol, F. F. Abdi, D. Friedrich, *et al.*, Extraction of mobile charge carrier photogeneration yield spectrum of ultrathin-film metal oxide photoanodes for solar water splitting, Nat. Mater. **20**, 833 (2021).

[26] C. Winnewisser, P. U. Jepsen, M. Schall, V. Schyja, and H. Helm, Electro-optic detection of THz radiation in $LiTaO_3$, $LiNbO_3$ and ZnTe, Appl. Phys. Lett. **70**, 3069 (1997).

[27] J. Neu, K. P. Regan, J. R. Swierk, and C. A. Schmuttenmaer, Applicability of the thin-film approximation in terahertz photoconductivity measurements, Appl. Phys. Lett. **113**, 233901 (2018).

[28] H. Hempel, C. J. Hages, R. Eichberger, I. Repins, and T. Unold, Minority and majority charge carrier mobility in $Cu_2ZnSnSe_4$ revealed by terahertz spectroscopy, Sci. Rep. **8**, 14476 (2018).

[29] M. Ziwritsch, S. Müller, H. Hempel, T. Unold, F. F. Abdi, R. van de Krol, D. Friedrich, and R. Eichberger, Direct time-resolved observation of carrier trapping and polaron conductivity in $BiVO_4$, ACS Energy Lett. **1**, 888 (2016).

[30] P. P. Infelta, M. P. de Haas, and J. M. Warman, The study of the transient conductivity of pulse irradiated dielectric liquids on a nanosecond timescale using microwaves, Radiat. Phys. Chem. **10**, 353 (1977).

[31] O. G. Reid, D. T. Moore, Z. Li, D. Zhao, Y. Yan, K. Zhu, and G. Rumbles, Quantitative analysis of time-resolved microwave conductivity data, J. Phys. D: Appl. Phys. **50**, 493002 (2017).

[32] G. F. McGuire, *Semiconductor Materials and Process Technology Handbook* (Elsevier Science, Stanford, 1988).

[33] D. Zhou, L. X. Pang, J. Guo, Z. M. Qi, T. Shao, Q. P. Wang, H. D. Xie, X. Yao, and C. A. Randall, Influence of Ce substitution for Bi in $BiVO_4$ and the impact on the phase evolution and microwave dielectric properties, Inorg. Chem. **53**, 1048 (2014).

[34] M. Kölbach, K. Harbauer, K. Ellmer, and R. Van De Krol, Elucidating the pulsed laser deposition process of $BiVO_4$ photoelectrodes for solar water splitting, J. Phys. Chem. C **124**, 4438 (2020).

[35] J.-W. Jang, D. Friedrich, S. Müller, M. Lamers, H. Hempel, S. Lardhi, Z. Cao, M. Harb, L. Cavallo, R. Heller, *et al.*, Enhancing charge carrier lifetime in metal oxide photoelectrodes through mild hydrogen treatment, Adv. Energy Mater. **7**, 1701536 (2017).

[36] M. Lamers, S. Fiechter, D. Friedrich, F. F. Abdi, and R. van de Krol, Formation and suppression of defects during heat treatment of $BiVO_4$ photoanodes for solar water splitting, J. Mater. Chem. A **6**, 18694 (2018).

[37] M. Kölbach, I. J. Pereira, K. Harbauer, P. Plate, K. Höflich, S. P. Berglund, D. Friedrich, R. Van De Krol, and F. F. Abdi, Revealing the performance-limiting factors in $\alpha - SnWO_4$ photoanodes for solar water splitting, Chem. Mater. **30**, 8322 (2018).

[38] E. D. Goodwin, D. B. Straus, E. A. Gaulding, C. B. Murray, and C. R. Kagan, The effects of inorganic surface treatments on photogenerated carrier mobility and lifetime in PbSe quantum dot thin films, Chem. Phys. **471**, 81 (2016).

[39] M. S. Prévot, X. A. Jeanbourquin, W. S. Bourée, F. Abdi, D. Friedrich, R. van de Krol, N. Guijarro, F. Le Formal, and K. Sivula, Evaluating charge carrier transport and surface states in $CuFeO_2$ photocathodes, Chem. Mater. **29**, 4952 (2017).

[40] M. Kölbach, H. Hempel, K. Harbauer, M. Schleuning, A. Petsiuk, K. Höflich, V. Deinhart, D. Friedrich, R. Eichberger, F. F. Abdi, *et al.*, Grain boundaries limit charge carrier transport in pulsed laser deposited $\alpha - SnWO_4$ thin film photoabsorbers, ACS Appl. Energy Mater. **3**, 4320 (2020).

[41] H. S. Han, S. Shin, D. H. Kim, I. J. Park, J. S. Kim, P. Huang, J. Lee, I. S. Cho, and X. Zheng, Boosting the solar water oxidation performance of a $BiVO_4$ photoanode by crystallographic orientation control, Energy Environ. Sci. **11**, 1299 (2018).

[42] Z. Zhao, Z. Li, and Z. Zou, Electronic structure and optical properties of monoclinic clinobisvanite $BiVO_4$, Phys. Chem. Chem. Phys. **13**, 4746 (2011).

[43] H. S. Han, S. Shin, D. H. Kim, I. J. Park, J. S. Kim, P.-S. Huang, J.-K. Lee, I. S. Cho, and X. Zheng, Boosting the solar water oxidation performance of a $BiVO_4$ photoanode by crystallographic orientation control, Energy Environ. Sci. **11**, 1299 (2018).

[44] F. F. Abdi, T. J. Savenije, M. M. May, B. Dam, and R. Van De Krol, The origin of slow carrier transport in $BiVO_4$ thin film photoanodes: A time-resolved microwave conductivity study, J. Phys. Chem. Lett. **4**, 2752 (2013).

[45] R. A. Street, *Hydrogenated Amorphous Silicon* (Cambridge University Press, Cambridge, 1991).

[46] O. Gabriel, S. Kirner, M. Klick, B. Stannowski, and R. Schlatmann, Plasma monitoring and PECVD process control in thin film silicon-based solar cell manufacturing, EPJ Photovoltaics **5**, 55202 (2014).

[47] L. Fekete, P. Kužel, H. Němec, F. Kadlec, A. Dejneka, J. Stuchlík, and A. Fejfar, Ultrafast carrier dynamics in microcrystalline silicon probed by time-resolved terahertz spectroscopy, Phys. Rev. B **79**, 115306 (2009).

[48] P. G. Le Comber and W. E. Spear, Electronic Transport in Amorphous Silicon Films, Phys. Rev. Lett. **25**, 509 (1970).

[49] R. A. Street, J. Kakalios, and M. Hack, Electron drift mobility in doped amorphous silicon, Phys. Rev. B **38**, 5603 (1988).

[50] P. G. Le Comber, D. I. Jones, and W. E. Spear, Hall effect and impurity conduction in substitutionally doped amorphous silicon, Philos. Mag. **35**, 1173 (1977).

[51] P. Grunow, D. Herm, R. Könenkamp, U. Küppers, M. Kunst, H. C. Neitzert, and A. Werner, The determination of the quality of *a*-Si : H Films for application in solar cells, MRS Proc. **149**, 363 (1989).

[52] A. Werner, M. Kunst, G. Beck, J. Lilie, and H. Tributsch, "*In situ*" measurements of the transient photoconductivity in *a*-Si : H, Solid State Commun. **56**, 127 (1985).

[53] J.-B. Chévrier, R. Vanderhaghen, C. Swiatkowski, H.-C. Neitzert, and M. Kunst, Carrier transport in *a*-Si : H/*a*-Si : N and *a*-Si : H/*a*-Si : C multilayers, J. Non-Cryst. Solids **164–166**, 837 (1993).

[54] A. R. Moore, in *Hydrogenated Amorphous Silicon*, edited by J. I. Pankove (Elsevier, Princeton, New Jersey, 1984), Vol. 21, p. 239.

[55] Y. Bi, E. M. Hutter, Y. Fang, Q. Dong, J. Huang, and T. J. Savenije, Charge Carrier Lifetimes Exceeding 15 μs in Methylammonium Lead Iodide Single Crystals (2016).

[56] J. Benick, A. Richter, M. Ralph, H. Hauser, F. Feldmann, P. Krenckel, S. Riepe, F. Schindler, M. C. Schubert, M. Hermle, *et al.*, High-efficiency *n*-type HP Mc silicon solar cells, IEEE J. Photovoltaics **7**, 1171 (2017).

[57] T. J. Magnanelli and E. J. Heilweil, Carrier mobility of silicon by sub-bandgap time-resolved terahertz spectroscopy, Opt. Express **28**, 7221 (2020).

[58] S. S. Li and W. R. Thurber, The dopant density and temperature dependence of electron mobility and resistivity in *n*-type silicon, Solid-State Electron. **20**, 609 (1977).

[59] J. M. Dorkel and P. Leturcq, Carrier mobilities in silicon semi-empirically related to temperature, doping and injection level, Solid-State Electron. **24**, 821 (1981).

[60] B. Michl, J. Benick, A. Richter, M. Bivour, J. Yong, R. Steeman, M. C. Schubert, and S. W. Glunz, Excellent average diffusion lengths of 600 μm of n-type multicrystalline silicon wafers after the full solar cell process including boron diffusion, Energy Procedia **33**, 41 (2013).

[61] T. Tiedje, B. Abeles, D. L. Morel, T. D. Moustakas, and C. R. Wronski, Electron drift mobility in hydrogenated a-Si, Appl. Phys. Lett. **36**, 695 (1980).

[62] A. D. Wright, R. L. Milot, G. E. Eperon, H. J. Snaith, M. B. Johnston, and L. M. Herz, Band-tail recombination in hybrid lead iodide perovskite, Adv. Funct. Mater. **27**, 1700860 (2017).

[63] P. Prins, F. C. Grozema, J. M. Schins, and L. D. A. Siebbeles, Frequency dependent mobility of charge carriers along polymer chains with finite length, Phys. Status Solidi **243**, 382 (2006).

[64] M. J. Bird, O. G. Reid, A. R. Cook, S. Asaoka, Y. Shibano, H. Imahori, G. Rumbles, and J. R. Miller, Mobility of holes in oligo- and polyfluorenes of defined lengths, J. Phys. Chem. C **118**, 6100 (2014).

[65] P. Kužel and H. Němec, Terahertz spectroscopy of nanomaterials: A close look at charge-carrier transport, Adv. Opt. Mater. **8**, 1900623 (2020).

[66] See the Supplemental Material at http://link.aps.org/supplemental/10.1103/PRXEnergy.1.023008 for discussions of "a"-factor determination, additional experimental data, methods, K-factor determination, influence of TRMC detector and injection level, sample preparation, literature comparison, and fitting method; Figures S1–S13; and Tables S1–S3.

[67] C. RØnne, L. Thrane, P.-O. Åstrand, A. Wallqvist, K. V. Mikkelsen, and S. R. Keiding, Investigation of the temperature dependence of dielectric relaxation in liquid water by THz reflection spectroscopy and molecular dynamics simulation, J. Chem. Phys. **107**, 5319 (1997).